Iraqi Journal of Science, 2026, Vol. 67, No. 4, pp: 2185-2197
DOI: 10.24996/ijs.2026.67.4.23

ISSN: 0067-2904

Biological Preparation of Iron-Zinc Oxides Core-Shell (Fe_3O_4-ZnO) Nanoparticles Using *Nerium oleander* Extracts and Their Activities Against *F. oxysporum f.sp. lycopersici*

M. J. Khadum *, L. A. Yaaqoob

Department of Biotechnology, Collage of Science, University of Baghdad, Iraq

Received: 24/11/2024 Accepted: 4/ 5 /2025 Published: 30/4/2026

Abstract

This study aimed to use Nerium oleander as a reducing and stabilizing agent for core-shell nanoparticles of iron and zinc (Fe_3O_4-ZnO) to use as an antimicrobial agent. The biosynthesized (Fe_3O_4-ZnO) NPs were characterized by various techniques such as UV-VIS, AFM, EDX, TEM, and Zeta potential. The wavelength of the (Fe_3O_4-ZnO) core-shell nanoparticles was (319 nm), the diameter was identified by atomic force microscopy (AFM), the average diameter was 78.74 nm, the core and shell nanoparticles (Fe_3O_4-ZnO) were confirmed by transmission electron microscopy (TEM) through the dark inner region representing the core and the bright part surrounding the dark region representing the shell and Zeta potential for (Fe_3O_4-ZnO) core-shell nanoparticles was 29.89- mV. For molecular diagnosis of *Fusarium oxysporum f.sp. lycopersici*, DNA was extracted to determine the identity of the isolate. The sample contained the target DNA fragments of 680 base pairs in size. The result was 100% identical in the NCBI GenBank database with *F. oxysporum*. The ITS rDNA sequence of the strain has been deposited in the NCBI GenBank database (GenBank accession numbers PQ060101). The antimicrobial activity of the core and shell nanoparticles (Fe_3O_4-ZnO) was recorded at 400 µg/mL with a maximum inhibition zone of 33 mm in diameter and minimum inhibition zone at 100 µg/mL with a diameter of 13 mm.

Keywords: *Nerium oleander*, core-shell, *Fusarium oxysporum f.sp. lycopersici,* molecular diagnosis, Antimicrobial.

التحضير البيولوجي لجسيمات نانوية من أكاسيد الحديد والزنك (Fe_3O_4– ZnO) باستخدام مستخلصات نبات الدفلى وفعاليتها ضد *F. oxysporum f.sp. lycopersici*

محمد جواد كاظم * ، ليث احمد يعقوب

قسم التقنيات ، كلية العلوم ، جامعة بغداد، بغداد، العراق

الخلاصة

هدفت هذه الدراسة إلى استخدام الدفلة كعامل اختزال وتثبيت للجسيمات النانوية ذات القشرة الأساسية من الحديد والزنك (Fe3O4– ZnO) واستخدامه كمضاد للميكروبات. تم تشخيص جزيئات الحديد والزنك (Fe3O4– ZnO) ذات القشرة النانوية التي تم تصنيعها حيويا بتقنيات مختلفة مثل UV–VIS وAFM

*Email: mohammed.jawad2306@sc.uobaghdad.edu.iq

وEDX وجهد زيتا والمجهر الإلكتروني النافذ. بواسطة مقياس الطيف الضوئي الطول الموجي (Fe3O4– ZnO) الجسيمات النانوية ذات القشرة الأساسية عند (319 نانومتر) ، تم التعرف على القطر بمجهر القوة الذرية (AFM) حيث بلغ متوسط القطر 87.74 نانومتر، كانت إمكانات زيتا للجسيمات النانوية ذات القشرة الأساسية (Fe3O4: ZnO) 29.89– مللي فولت , تم تأكيد لجسيمات النانو الأساسية والقشرية (Fe3O4– ZnO)المجهر الإلكتروني النافذ (TEM) من خلال المنطقة الداخلية الداكنة التي تمثل اللب والجزء الساطع المحيط بالمنطقة الداكنة التي تمثل القشرة. للتشخيص الجزيئي لـ *Fusarium oxysporum f.sp. lycopersici*، تم استخراج الحمض النووي لتحديد هوية العزل وجد أن العينة تحتوي على شظايا DNA بحجم 680 زوجًا أساسيًا. كانت النتيجة متطابقة بنسبة 100٪ في قاعدة بيانات NCBI GenBank ووجد أنها مع *F. oxysporum*. تم إيداع تسلسل ITS rDNA للسلالة في قاعدة بيانات NCBI GenBank أرقام الوصول (GenBank PQ060101) تم تسجيل النشاط المضاد للميكروبات لجسيمات النانو الأساسية والقشرية (Fe3O4– ZnO) عند 400 ميكروجرام / مل مع أقصى منطقة تثبيط بقطر (33 ملي) ومنطقة التثبيط الدنيا عند 100 ميكروجرام / مل بقطر (13 ملي).

1. Introduction

Nanotechnology is the study of enormously tiny structures, usually with sizes ranging from 1 to 100 nm [1]. Richard Feynman was credited with introducing the idea of nanotechnology in his remarks titled "There's Plenty of Room at the Bottom." Since different quantum effects often develop, objects confined inside nanoscale zones frequently exhibit behaviors very different from those in the bulk phase [2, 3]. Numerous scientific disciplines have acknowledged that countless combinations of atoms and molecules arranged in different ways at the nanoscale can result in an infinite number of different types of materials [4]. Two approaches are commonly utilized to synthesize nanomaterials: the top-down technique and the bottom-up approach. A top-down technique breaks a superstructure down to the atomic or molecule level. It is a subtractive method that uses mechanical or chemical techniques; a bulk substance is broken down and confined into small structures in this process. Attrition, milling, and mechanical grinding are a few top-down techniques. A bottom-up technique is utilized to synthesize nanoparticles, and it depends on strong adhesion between the base substratum and the surface layer. For many years, the physical and chemical fabrication of nanomaterials has confirmed detrimental hazardous consequences for humans. The researchers focus on environmentally friendly nanoparticle production by incorporating readily available metabolites into biological and plant extracts. The green synthesis of nanomaterials approach minimizes nanoparticles' harmful effects on humans and the environment while enhancing their biocompatibility [5, 6].

Nerium oleander L. (Apocynaceae) is a plant that grows naturally, and has been extensively widespread over the Mediterranean area. It grows well in sunny, humid conditions close to water flows. The primary usage of oleander is as an ornamental plant. This species' toxicity and therapeutic qualities have been well-documented since antiquity. In actuality, all plant parts are poisonous and can paralyze the heart, therefore causing death [7]. It has some advantageous properties besides being toxic, such as anticancerous, antimalarial, anti-inflammatory, hepatoprotective, and cardioprotective [8]. The oxidation and reduction ability of the oleander plant has also been exploited in the manufacture of nanoparticles [9, 10].

One of the most important diseases affecting the plants is Fusarium wilt, one of the most dangerous and widespread diseases that affect tomatoes and is caused by the pathogen *Fusarium oxysporum f.sp. Lycopersici* [11] . Fusarium wilt is an economically important disease affecting tomato plants wherever they are planted, whether in the field or greenhouses. Because the disease thrives in warm, humid environments, it lowers fruit quality and

decreases yields by 50–60%; for susceptible cultivars, the loss may be as high as 100% [12]. Molecular techniques have emerged as one of the most effective methods to identify the relationships between the fungal *F. oxysporum* and formae specials, differentiate them, detect their races, and assess the susceptibility and resistance of tomato varieties to disease. Through DNA sequence comparison, internal transcribed spacer (ITS) requirements can be identified for specific forms of the disease. To address these issues, newer technologies and strategies are constantly evolving. In view of this, one of the steps being taken is the introduction of nanomaterial-based products to revolutionize modern agricultural practices, as these materials possess novel physical and chemical properties that provide a distinct advantage in plant disease management. Hence, studies have been directed towards the use of bio-based green nanoparticles such as iron oxide nanoparticles and (Fe_3O_4-ZnO) core-shell nanoparticles effectively against plant pathogens for protection of various crops as an alternative to commercially available synthetic chemical pesticides, which exhibit higher toxicity to humans and have distinct properties such as high reaction rate and high surface area to mass ratio and enhance the Zn and Fe nano nutrient to the soil [13, 14].

2. Material and method

Leaves of Nerium oleander

Leaves of *Nerium oleander* were obtained locally from Baghdad City and diagnosed by assistant professor in plant biology Dr. Majid R. Majeed at the University of Baghdad, College of Science, Department of Biotechnology.

Preparation of leaves extract

According to Shawuti *et al.,* [15], with certain modifications, dried leaves of oleander that had been collected were thoroughly rinsed (three times) in distilled water. The leaves were powdered using a pestle and mortar after being shade-dried, 100 g of leaves powder dissolved in 1L of distilled water. The mixture was stirred for 24 h at 40 °C, then allowed to cool to room temperature before being filtered through Whatman no. 42 filter paper and centrifuged for 20 minutes at around 4000 rpm. After that, the leaves extract was put in a sterile container and kept at 4 °C.

Synthesis of (Iron-Zinc) oxides core-shell nanoparticles

In the first stage, according to Singh *et al.,* [16], with certain modifications, the co-precipitation technique was utilized to create iron oxide nanoparticles (Fe_3O_4 NPs). It was prepared by use oleander extracts for the biosynthesis of iron oxide nanoparticles, which involved adding ferric sulfate to oleander extract in a 0.5:10 g/ml ratio. The mixture was shaken overnight in a dark room. The solution, including iron nanoparticles, was separated, centrifuged at 5000 rpm for 10 minutes to concentrate it, washed twice with ethanol, and precipitated for another 30 minutes at a comparable speed. After that, it was oven-dried at 40 ˚C for 30 minutes to produce a brown-black powder and then kept in a dark container for further investigation. Preparing for the second stage utilized oleander extracts for the biosynthesis of (Iron-Zinc) oxides core-shell nanoparticles. The iron nanoparticles that were previously prepared were utilized to synthesize (Iron-Zinc) oxides core-shell nanoparticles. According to Alden and Yaaqoob [17], with certain modifications, which involved adding iron oxide nanoparticles in a 0.01:10 g/ml ratio and zinc acetate in a 0.5:10 g /ml ratio to oleander extract and adjusting the pH to 7, the mixture was shaken overnight in a dark room. The solution was separated, centrifuged at 5000 rpm for 10 minutes to concentrate it, washed with ethanol, and precipitated for another 30 minutes at a comparable speed. The precipitated nanoparticles were dried in an oven at 40 ˚C for 30 minutes. Finally, the black powder was sealed in a dark container for later usage and analysis.

Characterization of iron oxide and (Fe_3O_4- ZnO) core-shell nanoparticles

The synthesized nanoparticles were characterized through a UV-Vis spectrophotometer, atomic force microscopy, Energy-dispersive X-ray analysis, Zeta Potential, and Transmission Electron Microscope (TEM) for (Fe_3O_4- ZnO) core-shell NPs. Tests were conducted at the Chemical Analysis Center in Iraq, Baghdad, to confirm the identity, size, shape, and stability of the nanomaterials.

Isolation of pathogen

The fungal isolate utilized in this study (*Fusarium oxysporum*) was obtained from the Ministry of Agriculture / Plant Protection directorate / Agricultural Pest Diagnosis Department. The isolate was activated and grown on potato dextrose agar (PDA) medium, morphological characterization was performed, and molecular characterization was restored using the PCR technique.

DNA extraction

The pathogenic fungus was activated on PDA medium at 25°C by cultivating the dish with a fungal disc (0.5 cm) and after 7 days. The fungal hyphae were collected and then placed in test tubes. All this work was done inside the isolation chamber (laminar) and then stored in the refrigerator. Later, 100 mg of mycelium was utilized to extract DNA using the (ZR FUNGAL/BACTERIAL/ YEAST DNA MINIPREP)-kit according to the manufacturer's instructions.

Molecular characterization

A 1.5 µL of DNA and 2 µL of primers (1 µL of forward 5′-TCCGTAGGTGAACCTGCGG -3′ and 1 µL of reverse 5′ TCCTCCGCTTATTGATATGC-3′) was added into a small tube containing 5 µL of Taq PCR PreMix, and the volume was then completed to 25 µL by adding 16.5 µL of sterile deionized water. The tube was then mixed by Vortex. The tube was then placed in a Thermocycler to perform the Polymerase Chain Reaction (PCR). The amplification conditions included initial denaturation at 94°C (1 cycle for 5 minutes). Denaturation (94°C for 40 seconds), annealing (52°C for 40 seconds), and extension (72°C for 40 seconds) for 35 cycles, with final extension at 72°C (1 cycle for 7 minutes) [18].

DNA visualization

To diagnose DNA contamination in the reagents and verify amplicons, they were run simultaneously with a conventional DNA molecular weight indicator on an agarose gel (1%), 3 µl of the processor loading buffer was mixed with 5 µl of the fungal DNA before loading on the gel. The electrophoresis process was carried out with a 5 v\cm2 volt for 1.30 min. The electrophoresis results were visualized under UV light [19].

ITS analysis

The PCR product was sent to Biogen, a Korean company, for the nitrogenous base sequence. These sequences were compared to sequences of various global fungal isolates available at the National Center for Biotechnology Information (NCBI) using nucleotide BLAST in GenBank.

Antimicrobial activity

Agar well diffusion was utilized to assess the antimicrobial activity of biogenic iron oxide nanoparticles and (Fe_3O_4- ZnO) core-shell nanoparticles against *Fusarium oxysporum*. The McFarland turbidity standard of 0.5 was applied to the test microbial cultures, resulting in a

microbial suspension of $1.5*10^8$ colony-forming units (CFU/ml). Sterile L-rods were utilized to disseminate 100µl of microbial cultures on Mueller-Hinton agar plates, which were then placed into sterile Petri dishes for the antimicrobial investigations. Once the agar plates were seeded, three wells were pierced to allow biogenic nanomaterials to be put into them at three different concentrations: (100, 200, and 400) µg/ml. The plates were incubated for 72 h at 25 °C. Measurements in millimeters were made of the inhibition zones against the test organisms [20].

3. Results and Discussion

Crude extracts of Nerium oleander leaves

After the leaves were washed, dried, and ground into a powder, the Nerium oleander leaf extract was made. The powder was combined with distilled water. The description of the final extract revealed that the aqueous extract displayed a brown color. This result agrees with a previous study [21]. The first step in getting ready to biosynthesize Fe_3O_4 nanoparticles from the *Nerium oleander* extract agreed with Win *et al.,* [22].While the second step was utilizing *Nerium oleander* extract for the biosynthesis of iron and zinc (Fe_3O_4-ZnO) core-shell nanoparticles, according to Azizi *et al.,* [23]. After preparation, the precipitated nanoparticles were dried in an oven at 250°C, for characterization and use as an anti-bacterial agent. The results imply that Nerium oleander was capable of oxidation, reduction, and green synthesis of nanoparticles, which has been accomplished by utilizing environmentally and eco-friendly suitable extracts from the plant [24].

Characterization of iron oxide and (Fe3O4- ZnO) core-shell nanoparticle

Ultraviolet-visible (UV-VIS) spectroscopy

Using a UV-VIS scanning spectrophotometry that covered a wavelength range of 200-1000 nm, the absorbance of the core shell nanoparticles made of iron oxide and zinc oxide was determined. The scan of the Fe_3O_4-NPs spectra with the observed spectra at 292 nm is shown in Figure (1). This finding was in perfect harmony with prior research [25]. Another study has shown that the formation of Fe_3O_4 nanoparticles is attributed to a variety of plant biomolecules, which played a key role in the reduction of metal ions and contributed to the efficient stabilization of Fe_3O_4 nanoparticles. The UV-vis spectra of the synthesized nanoparticles showed absorption bands at low concentrations compared to those at high concentrations; when produced biologically, they had an absorption band between 230 and 290 nm [26].

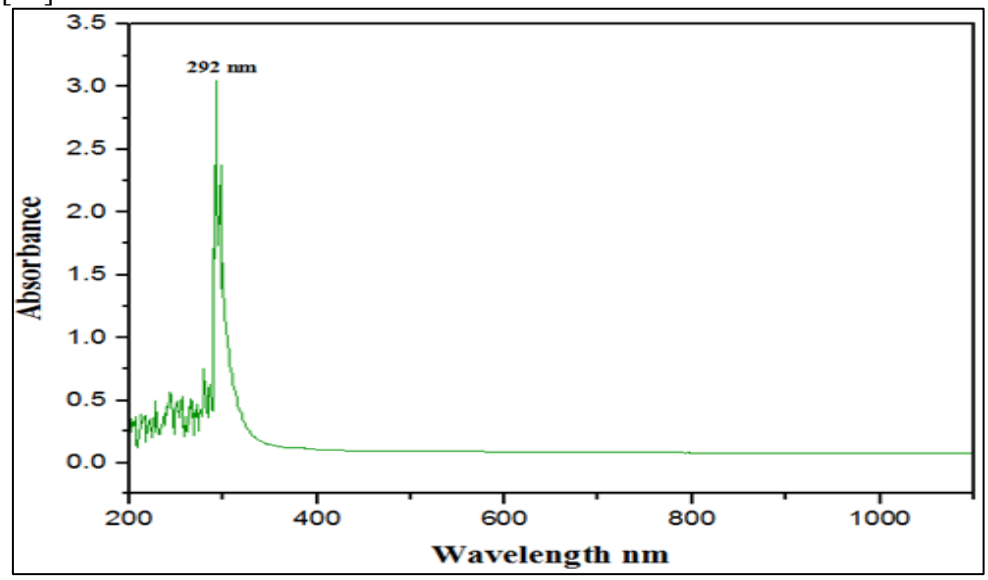

Figure 1: Spectra scan of iron oxide nanoparticle.

As shown in Figure 2, the scan of the (Fe_3O_4- ZnO)-NPs pattern, which was synthesised using the biological technique, can be identified at an absorbance spectrum of 319 nm. Consistent with earlier research using Tribulus seed powder for biological synthesis, this finding was very satisfactory [27]. The ability to identify (Fe3O4-ZnO)-NPs synthesised by chemical means with the absorption of 361 nm was shown in a separate work [28].

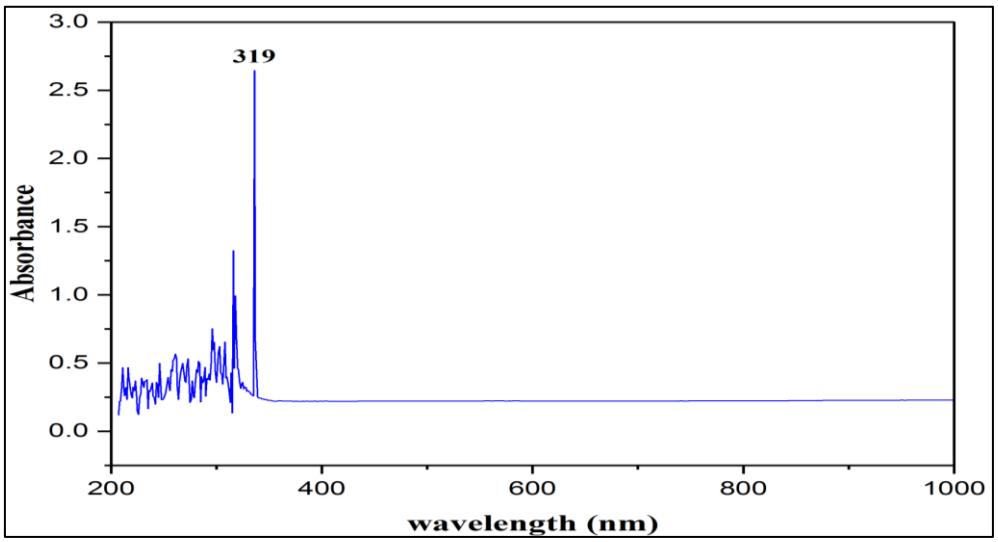

Figure 2: Spectra scan of (Fe3O4- ZnO) core-shell nanoparticle.

Atomic force microscopy (AFM)

Atomic force microscopy was utilized to investigate the surface shape formation of the iron oxide and (Fe_3O_4- ZnO) core-shell nanoparticle, the result demonstrating that the Fe_3O_4-NPs were spherical, as revealed by AFM images, 2D and 3D, as shown in Figure 3. The results also showed the average diameters of Fe_3O_4-NPs 24.99 nm, as shown in Table 1.

Table 1: The global statistics of iron oxide nanoparticles.

Global statistical	mean diameter
Mean	24.99
Min	2.820
Max	122.4

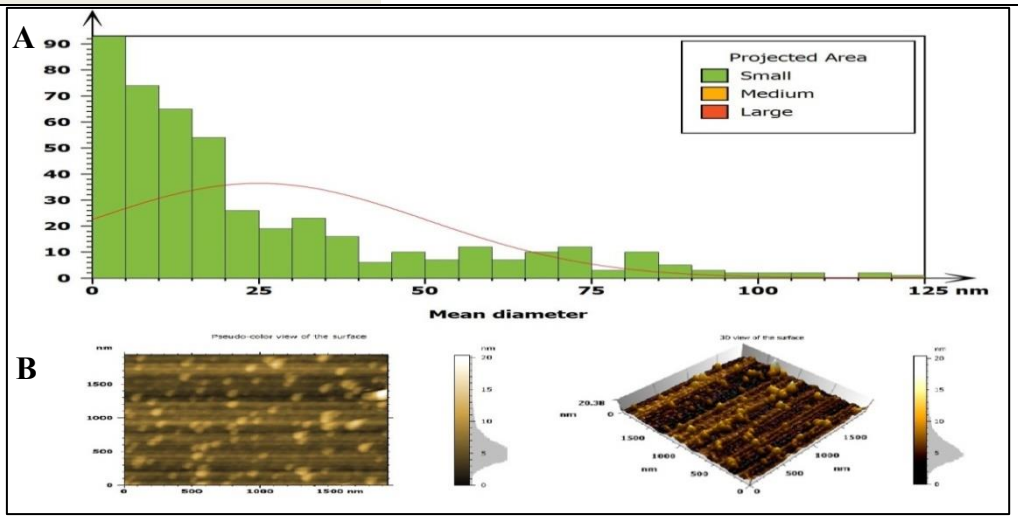

Figure 3: Atomic Force Microscopy of iron oxide NPs (A: Histogram of iron oxide NPs, B: 2D and 3D of iron oxide nanoparticles).

AFM images depicted the spherical morphology of the biosynthesized nanoparticles (NPs), as illustrated in Figure 4. The average diameter of (Fe3O4- ZnO) core-shell nanoparticles was found to be 78.74 nm, as shown in Table 2. This increase in diameter can be attributed to the incorporation of zinc, indicating a volumetric expansion. Furthermore, the packing density of zinc NPs is expected to rise with increased zinc acetate concentration, as evidenced by their abundance in the energy-dispersive X-ray (EDX) analysis, where it serves as a valuable tool for detecting nanoparticles. Additionally, the characterization of minerals.

Table 2: The global statistical of (Fe_3O_4- ZnO) core-shell nanoparticle.

Global statistical	mean diameter
Mean	78.74.
Min	8.753
Max	353.4

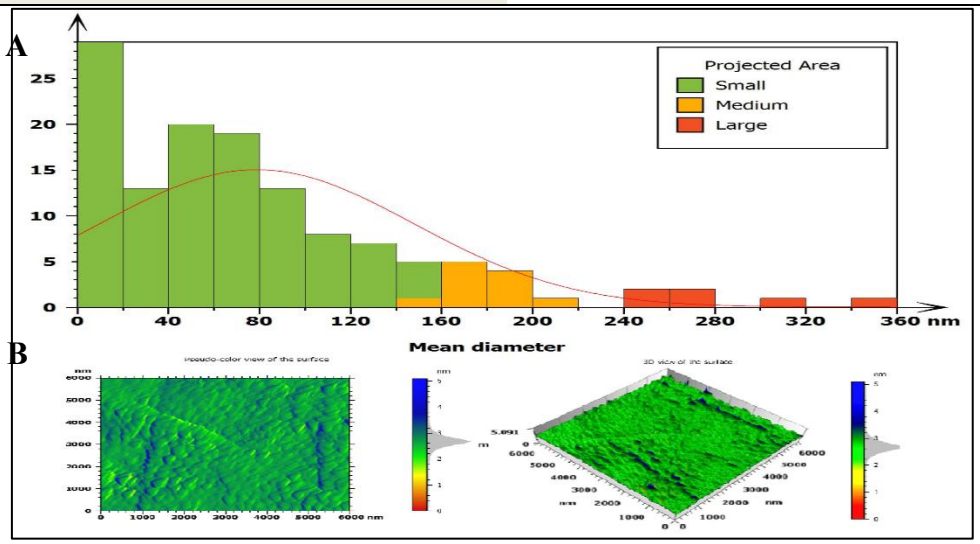

Figure 4: Atomic force microscopy (AFM) of (Fe_3O_4- ZnO) core-shell nanoparticles (A: Histogram of core shell-NPs, B: 2D and 3D of core shell-NPs).

Energy diffraction X- ray (EDX)

The result of this measurement is shown in Figure 5 and Table 3.

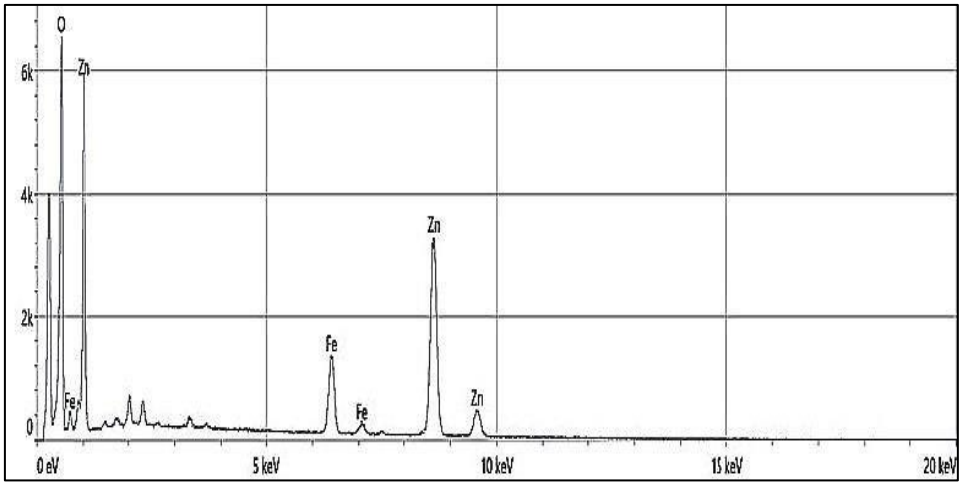

Figure 5: Energy diffraction X- ray (EDX) of (Fe_3O_4- ZnO) core-shell nanoparticles.

Table 3: Data analysis of EDX

Element	Atomic %
O	77.3
Fe	4.2
Zn	18.5

Transmission Electron Microscope (TEM)

This method depended on creating a high-intensity electron beam to which samples were exposed in order to capture photographs and analyze the material's microstructure using atomic-molecule analysis [29]. The TEM examination revealed two distinct zones, and when using a thinner sample, the observer typically sees through multiple atoms rather than one single atom. The production of (Fe_3O_4- ZnO) core-shell nanoparticles was confirmed by the dark inner area representing the core and the bright portion surrounding the dark region representing the shell. Iron and zinc TEM pictures are shown in Figure 6. A light color represents the shell, and the core by a dark color, agreed with Ameen *et al.,* [30].

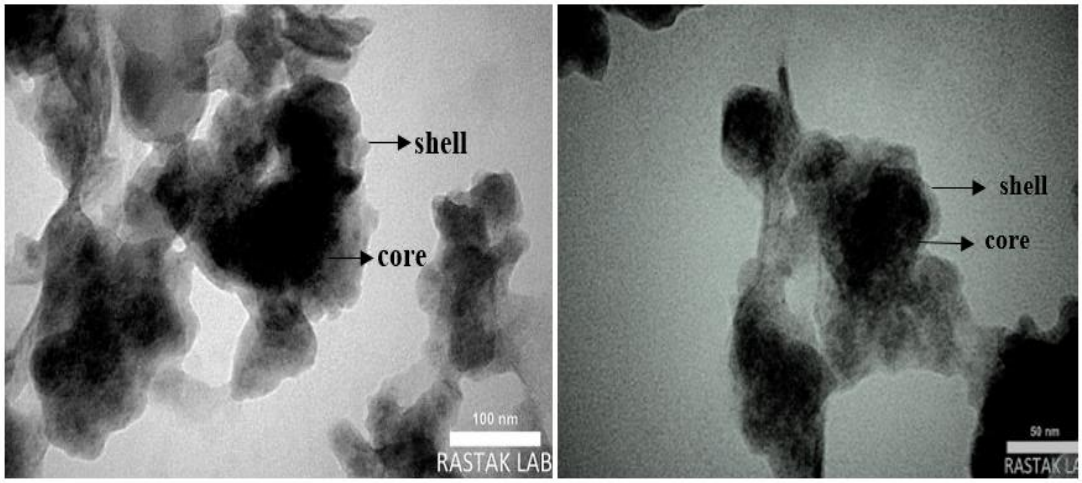

Figure 6: TEM images of iron and zinc (Fe_3O_4-ZnO) core-shell nanoparticles.

Zeta potential

It is common practice to measure the amount of an electrical charge using the zeta potential. Figure 7 shows that the average zeta potential of Fe3O4-NP is 20.9 mV. This result agrees with previous study [31] . Another study showed that the stability range of metal oxide (20 to 40 mV) [32].

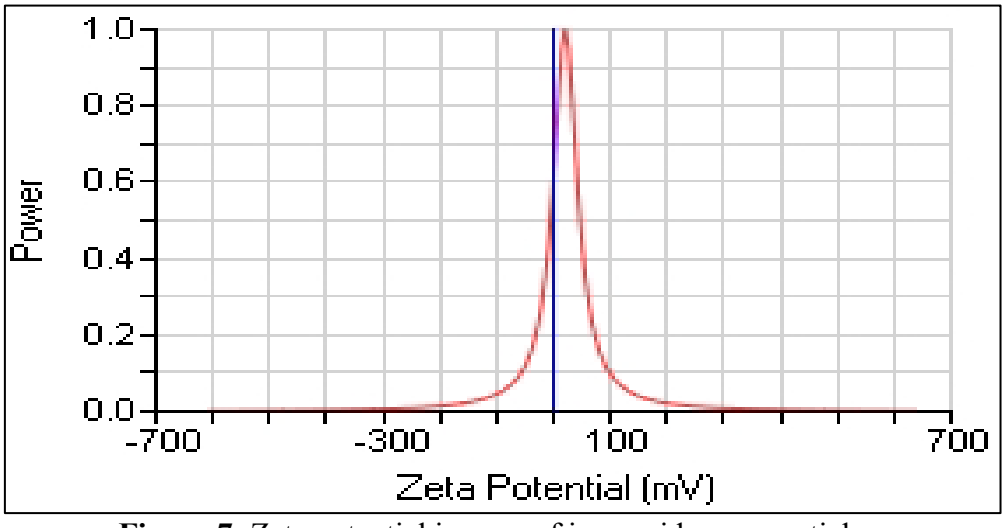

Figure 7: Zeta potential images of iron oxide nanoparticles.

While the average zeta potential of (Fe_3O_4- ZnO) core-shell nanoparticles was found to be -29.89 mV, as shown in Figure 8, this result agreed with previous study [33].

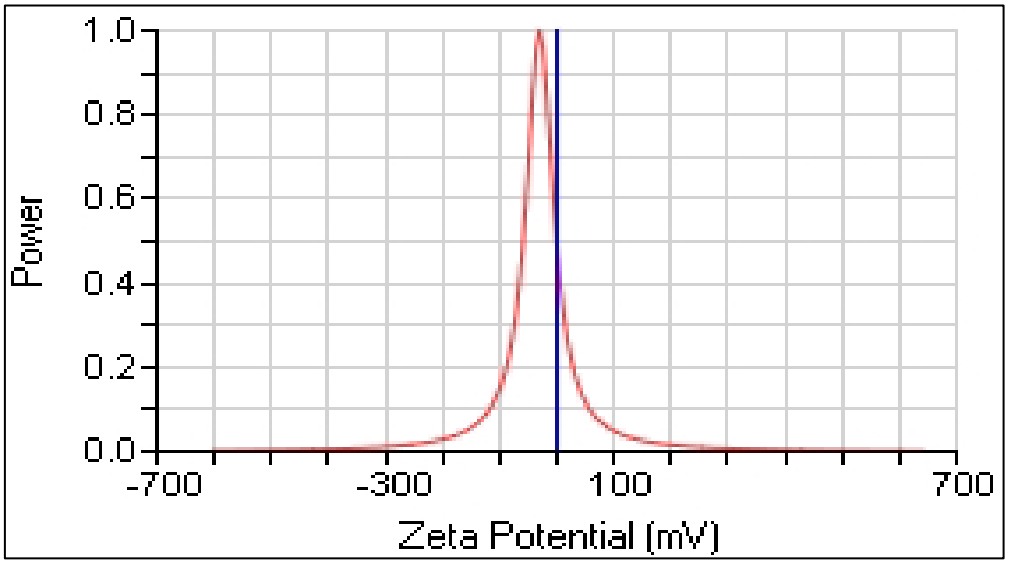

Figure 8: Zeta potential images of (Fe_3O_4- ZnO) core-shell nanoparticles.

DNA visualization and ITS analysis

Figure 9 shows that 680 bp amplicon was produced by PCR amplification of the isolate's ITS region.

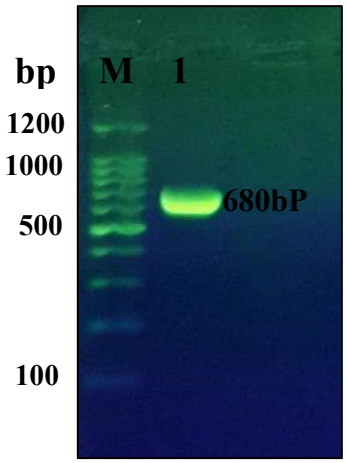

Figure 9: PCR product the band size 650 bp. The product was electrophoresis on 1% agarose at 5 volt/cm^2. 1x TBE buffer for 1:30 hours. M: DNA ladder (100).

The strain was identified by sequencing its ITS region. The results showed that *F. oxysporum f.sp. lycopersici* was 100% comparable to *F. oxysporum* in the NCBI GenBank database. The ITS rDNA sequencing of this strain has been submitted to the GenBank database at the National Centre for Biotechnology Information (GenBank Accession numbers PQ060101). This finding is consistent with earlier research on the detection and transportation of infectious fungal infections [34, 35].

Estimation of antifungals effect of (Fe_3O_4- ZnO) core-shell nanoparticles in comparison with Fe3O4 nanoparticles separately

The potential of iron oxide nanoparticles and (Fe_3O_4- ZnO) core-shell nanoparticles to inhibit the growth of *F. oxysporum*. The antifungal activity of NPs is shown in Figure 10. It was directly influenced by the concentrations of NPs. The concentration of iron oxide and (Fe_3O_4- ZnO) core-shell nanoparticles at 400 µg/ml produced a maximum inhibition zone of (19, 33) mm, respectively. On the other hand, the minimum inhibition zone was found at 100 µg/ml iron oxide (10) mm, and the (Fe_3O_4-ZnO) core-shell minimum inhibition zone was at concentrations of 100 µg/ml (13) mm, as shown in Table 4, the results demonstrated that the antifungal activity of each investigated NP increased significantly with concentration. Additionally, the antifungal activity of core-shell nanoparticles was found to be superior to that of iron oxide nanoparticles at all concentrations of iron oxide.

Table 4: The inhibition zone of Antifungal effect for iron oxide nanoparticles and (Fe_3O_4-ZnO) core-shell nanoparticles against nanoparticles against *F. oxysporum f.sp. lycopersici.*

Zone inhibition (in mm)			
NO	**Concentrations µg/ml**	**Fe_3O_4-NPs**	**(Fe_3O_4- ZnO)-NPs**
1	100	10	13
2	200	14	18
3	400	19	33

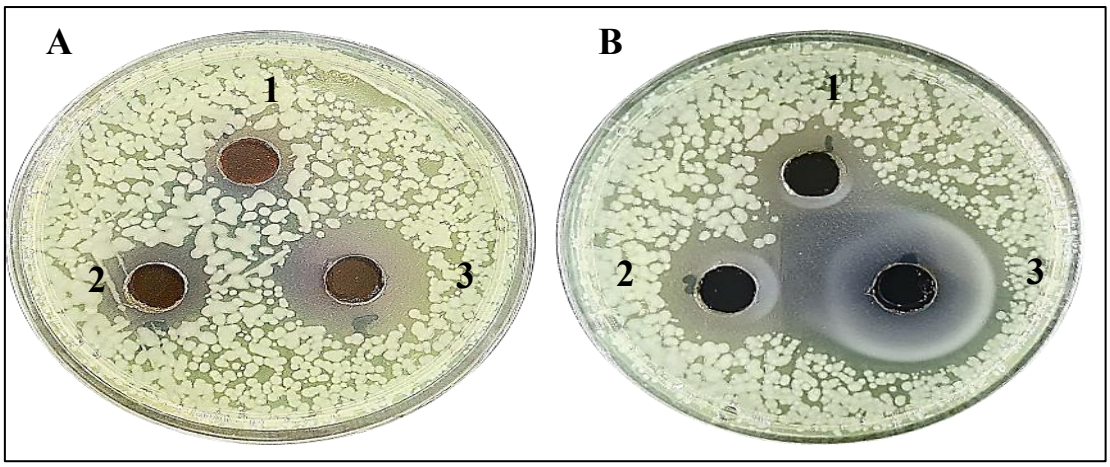

Figure 10: Antifungal activity: (A) zone inhibition of iron oxide nanoparticles, (B) inhibition zone of (Fe_3O_4- ZnO) core-shell nanoparticles.

Iron oxide, frequently referred to as hematite, has been demonstrated to eliminate microbes by osmosis and to be resistant to the body's acidity. In addition to reactive oxygen species (ROS), the interaction between iron oxide nanoparticles and hydrogen peroxide in the cells results in the production of hydroxyl and peroxide free radicals [36].The principal method by which ZnO NPs induce adverse effects on microbes is the generation ROS. The deterioration of biological elements, including DNA, lipids, and proteins, in particular, adds to the toxicity of ROS on the cell membrane. The majority agree that the primary cause of antimicrobial activity associated with ZnO photo-toxicity is the production of ROS. This ultimately causes oxidation, which either kills or inhibits the microbes [37]. Nanoparticles possess the ability to penetrate membranes, interfere with DNA replication, and act as catalysts to deactivate enzymes necessary for microbes' metabolism. Higher surface-to-volume ratio metal nanoparticles displayed maximum antimicrobial activity [38]. The inhibition effect of nanoparticles on pathogenic fungi is attributed to their large surface area, which allows them to come into greater contact with microorganisms, and their small size, which enables them to penetrate the cell wall easily. Nanoparticles cause deformation and swelling of the fungal cell

wall, leading to its disintegration, resulting in cytoplasm leakage out of the cells and fungal death [39].

5. Conclusion

The results of this study were to produce nanoparticles of iron oxide and core-shell (Fe_3O_4- ZnO) by incorporating metabolites readily available in plant extracts (Nerium oleander) and characterize each of them individually by advanced a UV-Vis, AFM, EDX, TEM and Zeta Potential. Study the effectiveness of the nanomaterials on *F. oxysporum f.sp. lycopersici* after genetic diagnosis (GenBank accession numbers PQ060101). The (Fe_3O_4-ZnO) core-shell nanoparticles have more positive results than iron oxide in terms of fungal inhibition. In future studies, core-shell should be used as an alternative to fungicides, and the effects of its use on plants should be studied, as it consists of zinc and iron, which are considered micro-fertilizer elements.

Ethical Clearance

The research stated in this study was approved by the Biotechnology Department's local committee. Researchers from Baghdad University conducted the research.

Conflict of Interest

The writers do not have any financial conflicts of interest.

References:

[1] S. N. Mazhir, N. F. Majeed, E. M. Abbas, and S. A. Qasim, "Synthesis of Green Zno/Fe3O4 Nanocomposite by Microplasma Jet and Anti-Bacterial Agent," *Iraqi Journal of Science*, vol. 64, no. 12, pp. 6215-6225, 2023.

[2] N. Mohammed, S. H. Nawar, M. S. Etawy, G. E. Nassar, and A. G. Hassabo, "Nanotechnology and its applications in industry and product design," *Journal of Textiles, Coloration and Polymer Science,* vol. 21, no. 2, pp. 273-284, 2024.

[3] A. S. Noori, K. A. Aadim, and A. H. Hussein, "Investigate and Prepare silver Nano Particles Using Jet Plasma," *Iraqi Journal of Science*, pp. 2461-2469, 2022.

[4] K. Ariga, "Nanoarchitectonics: what's coming next after nanotechnology?," *Nanoscale Horizons,* vol. 6, no. 5, pp. 364-378, 2021.

[5] P. Aarthye, and M. Sureshkumar, "Green synthesis of nanomaterials: An overview," *Materials Today: Proceedings,* vol. 47, pp. 907-913, 2021.

[6] M. A. Atiya, A. K. Hassan, and F. Q. Kadhim, "Green synthesis of copper nanoparticles using tea leaves extract to remove ciprofloxacin (CIP) from aqueous media," *Iraqi Journal of Science*, vol. 62, no. 9, pp. 2832-2854, 2021.

[7] K. Aberkani, A. Nafis, Z. Zgourdeh, A. Benchahid, H. Hanine, and S. E.-d. Samri, "Ethnobotanical study of medicinal plants used for cancer treatment at the province of Nador, Morocco," *Boletín Latinoamericano y del Caribe de Plantas Medicinales y Aromáticas,* vol. 23, no. 2, pp. 326-335, 2024.

[8] K. Chaudhary, V. B. Kushwaha, and S. K. Srivastav, "A REVIEW: NERIUM INDICUM OR NERIUM OLEANDER AND ITS TOXICITY IN VERTEBRATES," *system,* vol. 4, pp. 5, 2024.

[9] J. R. Bikkavolu, S. Vadapalli, K. R. R. Chebattina, and G. Pullagura, "Effects of stably dispersed carbon nanotube additives in yellow oleander methyl ester-diesel blend on the performance, combustion, and emission characteristics of a CI engine," *Biofuels,* vol. 15, no. 1, pp. 67-80, 2024.

[10] A. M. Shawky, R. Elshypany, H. M. El Sharkawy, M. F. Mubarak, and H. Selim, "Emerald eco-synthesis: harnessing oleander for green silver nanoparticle production and advancing photocatalytic MB degradation with TiO2&CuO nanocomposite," *Scientific Reports,* vol. 14, no. 1, pp. 2456, 2024.

[11] M. M. El-Sheekh, A. S. H. Mousa, and A. A. Farghl, "Biological control of Fusarium wilt disease of tomato plants using seaweed extracts," *Arabian Journal for Science and Engineering,* vol. 45, pp. 4557-4570, 2020.

[12] S. P. López-Zapata, D. J. García-Jaramillo, W. R. López, and N. Ceballos-Aguirre, "Tomato (Solanum lycopersicum L.) and *Fusarium oxysporum f. sp. lycopersici* interaction. A review," *Revista UDCA Actualidad & Divulgación Científica,* vol. 24, no. 1, 2021.

[13] D. Mittal, G. Kaur, P. Singh, K. Yadav, and S. A. Ali, "Nanoparticle-based sustainable agriculture and food science: Recent advances and future outlook," *Frontiers in Nanotechnology,* vol. 2, pp. 579954, 2020.

[14] S. Jehan, S. A. Khattak, M. Waqas, S. Khan, and L. Ali, "Evaluation Health Risks and Sorption of Hexavalent Chromium (Cr (VI) by Biochar and Iron Doped Zinc Oxide Modified Biochar (Fe-ZnO@ BC) Using Trifolium: A Green Synthesis Technique," *Bulletin of Environmental Contamination and Toxicology,* vol. 112, no. 4, pp. 54, 2024.

[15] S. Shawuti, C. Bairam, A. Beyatlı, İ. A. Kariper, I. N. Korkut, Z. Aktaş, M. O. Öncül, and S. E. Kuruca, "Green synthesis and characterization of silver and iron nanoparticles using Nerium oleander extracts and their anti-bacterial and anticancer activities," *Plant introduction*, no. 91/92, pp. 36-49, 2021.

[16] K. Singh, D. Sethi Chopra, D. Singh, and N. Singh, "Green synthesis and characterization of iron oxide nanoparticles using Coriandrum sativum L. leaf extract," *Indian Journal of Biochemistry and Biophysics (IJBB),* vol. 59, no. 4, pp. 450-454, 2022.

[17] U. R. Hameed, and L. Yaaqoob, "Antibacterial activity of cobalt and titanium (Co-Tio2) Core-shell nanoparticles against *Escherichia coli* isolates from deferent sources," *Iraqi Journal of Biotechnology*, vol. 21, no. 2, pp 341-357, 2022.

[18] M. Zarrin, F. Ganj, and S. Faramarzi, "Analysis of the rDNA internal transcribed spacer region of the Fusarium species by polymerase chain reaction-restriction fragment length polymorphism," *Biomedical Reports,* vol. 4, no. 4, pp. 471-474, 2016.

[19] M. F. Arif, A. D. Prasetya, I. Lesmana, and N. S. N. Handayani, "Comparison of Lysis Buffers for Saliva DNA Extraction using Modified Magnetic-Silica Nanoparticle Beads," *Biotropika: Journal of Tropical Biology,* vol. 11, no. 1, pp. 1-8, 2023.

[20] J. V. Perez, L. Serrano, R. Viteri, D. Sosa, C. A. Romero, and N. Diez, "Antarctic Streptomyces: Promising biocontrol agents for combating *Fusarium oxysporum f. sp*. cubense," *Biotechnology Reports,* vol. 43, pp. e00852, 2024.

[21] H. M. Albert, and C. A. Gonsago, "Green Procedure for the synthesis of Copper Nanoparticles using Nerium oleander Leaf Extract: Characterizations and Applications," *Oriental Journal of Chemistry,* vol. 39, no. 3, 2023.

[22] T. T. Win, S. Khan, B. Bo, S. Zada, and P. Fu, "Green synthesis and characterization of Fe3O4 nanoparticles using Chlorella-K01 extract for potential enhancement of plant growth stimulating and antifungal activity," *Scientific Reports,* vol. 11, no. 1, pp. 21996, 2021.

[23] Z. Azizi, M. Ghazvini, S. Afrashteh, and Z. Hossaini, "Green Synthesis and Theoretical Study of New Azepinodiazepine Derivatives with Biological Activity: Application of Fe3O4/ZnO@ MWCNT," *Polycyclic Aromatic Compounds,* vol. 44, no. 4, pp. 2508-2534, 2024.

[24] S. Vijayaram, H. Razafindralambo, Y.-Z. Sun, S. Vasantharaj, H. Ghafarifarsani, S. H. Hoseinifar, and M. Raeeszadeh, "Applications of green synthesized metal nanoparticles—a review," *Biological Trace Element Research,* vol. 202, no. 1, pp. 360-386, 2024.

[25] V. Niraimathee, V. Subha, R. E. Ravindran, and S. Renganathan, "Green synthesis of iron oxide nanoparticles from Mimosa pudica root extract," *International Journal of Environment and Sustainable Development,* vol. 15, no. 3, pp. 227-240, 2016.

[26] A. Hussain, M. Yasar, G. Ahmad, M. Ijaz, A. Aziz, M. G. Nawaz, F. A. Khan, H. Iqbal, W. Shakeel, and H. Momand, "Synthesis, characterization, and applications of iron oxide nanoparticles," *International Journal of Health Sciences,* vol. 17, no. 4, pp. 3, 2023.

[27] K. Vanitha Bharathi, M. N. Meeran, and R. Kayalvizhi, "Tribulus terrestrias synthesized Fe3O4/ZnO nanocomposites for ultra-rapid methyl orange elimination using ultrasonic waves," *Biomass Conversion and Biorefinery*, pp. 1-13, 2024.

[28] J. C. B. Huarac, M. Tomar, S. Singh, O. Perales-Perez, L. Rivera, and S. Pena, "Multifunctional Fe3O4/ZnO core-shell nanoparticles for photodynamic therapy." *In NSTI-Nanotech*, vol. 3, pp. 405-408, 2010.

[29] A. Azor-Lafarga, I. Gómez-Recio, M. L. Ruiz-González, and J. M. González-Calbet, "Atomic Resolution Electron Microscopy: A Key Tool for Understanding the Activity of Nano-Oxides for Biomedical Applications," *Nanomaterials,* vol. 11, no. 8, pp. 2073, 2021.

[30] F. Ameen, E. E. Altuner, R. N. E. Tiri, F. Gulbagca, A. Aygun, F. Sen, N. Majrashi, R. Orfali, and E. N. Dragoi, "Highly active iron (II) oxide-zinc oxide nanocomposite synthesized Thymus vulgaris plant as bioreduction catalyst: Characterization, hydrogen evolution and photocatalytic degradation," *International Journal of Hydrogen Energy,* vol. 48, no. 55, pp. 21139-21151, 2023.

[31] P. Ma, Q. Luo, J. Chen, Y. Gan, J. Du, S. Ding, Z. Xi, and X. Yang, "Intraperitoneal injection of magnetic Fe3O4-nanoparticle induces hepatic and renal tissue injury via oxidative stress in mice," *International journal of nanomedicine*, pp. 4809-4818, 2012.

[32] N. Sizochenko, A. Mikolajczyk, M. Syzochenko, T. Puzyn, and J. Leszczynski, "Zeta potentials (ζ) of metal oxide nanoparticles: A meta-analysis of experimental data and a predictive neural networks modeling," *NanoImpact,* vol. 22, pp. 100317, 2021.

[33] H. S. Abbas, A. Krishnan, and M. Kotakonda, "Fabrication of iron oxide/zinc oxide nanocomposite using creeper Blepharis maderaspatensis extract and their antimicrobial activity," *Frontiers in Bioengineering and Biotechnology,* vol. 8, pp. 595161, 2020.

[34] S. Deng, W. Chang, Q. Liu, Y. Zhao, J. Liu, and H. Wang, "Development and application of multiplex PCR for the rapid identification of four Fusarium spp. associated with Fusarium crown rot in wheat," *PeerJ,* vol. 12, pp. e17656, 2024.

[35] L. Murugan, N. Krishnan, V. Venkataravanappa, S. Saha, A. Mishra, B. Sharma, and A. Rai, "Molecular characterization and race identification of *Fusarium oxysporum f. sp*. lycopersici infecting tomato in India," *3 Biotech,* vol. 10, pp. 1-12, 2020.

[36] L. Lai, Y. He, H. Zhou, B. Huang, G. Yao, and B. Lai, "Critical review of natural iron-based minerals used as heterogeneous catalysts in peroxide activation processes: Characteristics, applications and mechanisms," *Journal of Hazardous Materials,* vol. 416, pp. 125809, 2021.

[37] C. R. Mendes, G. Dilarri, C. F. Forsan, V. d. M. R. Sapata, P. R. M. Lopes, P. B. de Moraes, R. N. Montagnolli, H. Ferreira, and E. D. Bidoia, "Anti-bacterial action and target mechanisms of zinc oxide nanoparticles against bacterial pathogens," *Scientific reports,* vol. 12, no. 1, pp. 2658, 2022.

[38] F. Buarki, H. AbuHassan, F. Al Hannan, and F. Henari, "Green synthesis of iron oxide nanoparticles using Hibiscus rosa sinensis flowers and their anti-bacterial activity," *Journal of Nanotechnology,* vol. 2022, no. 1, pp. 5474645, 2022.

[39] Y. N. Slavin, and H. Bach, "Mechanisms of antifungal properties of metal nanoparticles," *Nanomaterials,* vol. 12, no. 24, pp. 4470, 2022.